



Test of Novel Self-Centering Energy Dissipative Braces with Pre-Pressed Disc Springs and U-Shaped Steel Plates

Junfeng Jia^a, Ranxing Gu^a, Canxing Qiu^a, Tianyi Huang^a, Binli Guo^b, and He Guo^c

^aKey Laboratory of Urban Security and Disaster Engineering of Ministry of Education, Beijing University of Technology, Beijing, China; ^bCCCC Infrastructure Maintenance Group Co., LTD., Beijing, China; ^cCCCC Road & Bridge Inspection & Maintenance Co., LTD., Beijing, China

ABSTRACT

To control the residual displacement of the structure after strong earthquakes, this paper develops and validates a novel brace, i.e. the self-centering energy dissipative brace with pre-pressed disc springs and U-shaped steel plates (SCEDB-U). The pre-pressed disc springs are used for recovering nonlinear deformation and the U-shaped steel plates are used for dissipating energy. Initially, the configuration and working principle are described in detail. Then the analytical equations governing the cyclic behavior of the brace are derived. To confirm the concept, the large-scale bracing specimens are designed and manufactured for the quasi-static cyclic loading tests. In the tests, the varied parameters included the plate width of the U-shaped steel plates and the pre-pressure magnitude of the stacked disc springs. Besides, the high-fidelity three-dimensional finite element (FE) models of SCEDB-U are established. According to the experimental data, the SCEDB-U has typical flag-shaped hysteresis, which is characterized by excellent self-centering capability and stable energy dissipation ability. It also indicates that increasing the plate width of U-shaped steel plates can effectively improve the energy dissipation capacity, but may induce residual displacement; increasing the pre-pressure magnitude of disc springs could improve self-centering ability. The numerical results are in good agreement with the experimental data; hence, the FE models can be further utilized for parametric analysis, initial design and optimization.

ARTICLE HISTORY

Received 18 May 2022

Accepted 21 November 2022

KEYWORDS

Self-centering brace;
U-shaped steel plate; disc
spring; experimental test;
cyclic behavior

1. Introduction

Ordinary steel braces are often used in practical constructions due to simple configuration and convenient installation, but they are prone to buckling-induced instability upon compression actions, which results in rapid capacity degradation of strength, ductility and energy dissipation (Christopoulos et al. 2008; Fell et al. 2009). To address the issue, the community proposed buckling-restrained braces (BRBs), which confine the tension-compression steel core into buckling-restrained devices. Accordingly, BRBs could provide full energy dissipation capacity and have significantly improved fatigue performance, and they have been successfully applied to reduce seismic responses of structures, mainly for collapse prevention purpose (Bai et al. 2021; Ghowzi and Sahoo 2022; Sabelli, Mahin, and Chang 2003). However, the community has noticed that BRBs are not that effective in reducing residual deformations for the protected structures (Qiu et al. 2018; Tremblay, Lacerte, and Christopoulos 2008). Excessive residual deformations raise seismic loss and impede the post-event recovery, and decrease seismic resilience (Ramirez and Miranda 2012).

Toward controlling or even eliminating residual deformations of the structures, the community introduced self-centering (SC) elements and proposed a variety of SC energy dissipative (ED) braces (SCEDBs) in recent years. In the early stage, the post-tensioned (PT) rebars/tendons/strands are often used as the SC elements. Representatives included the aramid fiber tendons (Christopoulos et al. 2008), high-strength steel rebars and strands (Wang, Nie, and Pan 2017), and FRPs (Wang et al. 2021). The elastic deformation capacity of these PT components is very limited, and the researchers had proposed the telescoping or dual core device to double the stroke of the SCEDBs (Erochko, Christopoulos, and Tremblay 2015). However, the details of the PT-based SCEDBs are very demanding. Besides, anchoring PT components is very challengeable and the prestressing level may lose (Fang et al. 2022). Shape memory alloy (SMA) based components are another promising SC candidate for developing SCEDBs, which can be found in many earlier studies (Fang et al. 2018, 2020; Qiu and Zhu 2017; Qiu et al. 2020; Qiu, Liu, and Du 2022), but the high material price and the sensitivity to temperature change should be kept in mind. As an alternative, the disc springs are increasingly favored by the community, due to large deformation stroke, concise configuration, and stable properties (Fang, Wang, and Shen 2021). In fact, a variety of SCEDBs using disc springs have been developed and experimentally confirmed, such as those by Xu, Fan, and Li (2016), Dong et al. (2019), and Huang et al. (2019).

Besides with exploring the SC elements, the community paid great efforts in selecting the ED devices. In summary of the existing studies, the ED devices adopted by SCEDBs mainly included the friction mechanisms (Christopoulos et al. 2008), viscous damping materials (Zhu et al. 2020), and metallic yielding devices (Qiu et al. 2020). Friction devices have efficient damping mechanism even under small deformations, but the abrasion may change the coefficient of kinetic friction (Jaisee, Yue, and Ooi 2021). Regarding the viscous damping materials, the common issue is they are lack of sufficient strength and leakage issue (Kumar and Kumar 2021). Metallic yielding devices have various configurations, such as the steel bending plates (Qiu et al. 2020), steel angles (Wang, Fang, and Liu 2017) and steel BRBs (Dong et al. 2019), but the corresponding problems are the limited deformation capacity, complex cyclic behavior, and asymmetrical tension and compression hysteresis, respectively.

Recently, the metallic dampers using U-shaped steel plates have attracted increasing attentions, due to stable hysteresis, high damping and large deformation capability. For example, Deng et al. (2015) and Deng, Pan, and Wang (2013). experimentally tested a crawler steel damper using U-shape steel plates, which exhibited full hysteresis and excellent the deformation capacity. Jiao et al. (2015). further confirmed the observations through extensive loading tests. The major applications of U-shaped steel plates are for the isolation system (Jiao et al. 2015), whereas they are rarely utilized in braces. The experimental work conducted by Qu et al. (2019). and Taiyari, Mazzolani, and Bagheri (2019). validated the feasibility. In the tests, both braces exhibited full, stable, and symmetrical hysteresis, whereas the residual deformation is noticeable.

Therefore, in recognition of the merits of disc springs and U-shaped steel plates, this paper proposes a novel SCEDB, i.e. the SCEDB with pre-pressed disc springs and U-shaped steel plates (SCEDB-U). The stacked pre-pressed disc springs are used as SC element and several groups of U-shaped steel plates are used as ED element. The brace has a simple yet concise configuration, which permits easy inspection after earthquakes and allows to repair and replace the damaged elements, if necessary. It firstly describes the configuration and working principle of the SCEDB-U. And then, the analytical equations governing the cyclic behavior are derived. To examine the concept, three full-scale bracing specimens are fabricated for cyclic loading tests, in which the varied parameters include the plate width of the U-shaped steel plates and the pre-pressure magnitude of the disc springs. Finally, three-dimensional finite element (FE) models are established to further unveil the behavior of the SCEDB-U and provide a basis for future parametric analysis and design.

2. Working Principle of the SCEDB-U

As shown in Fig. 1, the SCEDB-U is composed of force transmission system, ED system and SC system. Specifically, the ED system is mainly composed of several pairs of U-shaped steel plates, which

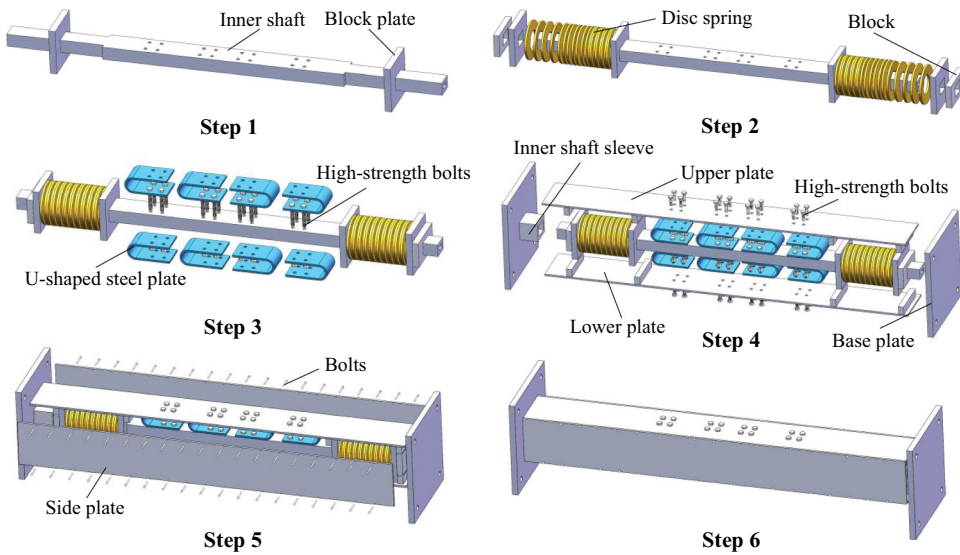


Figure 1. Configuration and fabrication steps of the SCEDB-U.

are arranged between the inner shaft and the covering plates through bolting connection. The SC system is offered by the stacked disc springs which are prepressed to target level by the block plates. The force transmission system includes inner shaft, covering plates, block plates, inner tube sleeve, base plates at both ends, and the other accessories. The inner shaft passes throughout the prepressed disc springs. One end of the inner shaft is welded to the base plate, and the other end is freely floating in the sleeve. The inner shaft and covering plates have suitable space for accommodating the U-shaped steel plates and disc springs. The inner shaft is shaped into a stepped section from a customized steel tube, which acts as the guiding component of the ED and SC systems. There are four covering plates, in which the upper and lower plates are bolted with the U-shaped steel plates, and two side plates are bolted with the upper and lower plates. One end of the covering plates is welded to the base plate and the other end is free from constraint. The assembly manner can facilitate inspection and replacement of the damaged elements after strong earthquakes, if necessary.

The basic deformation mode is presented in Fig. 2, including the at-rest position, the tensioned position and compressed position. Initially, the pre-pressed disc springs are firmly restricted by the block plates, and meanwhile, the U-shaped steel plates are under zero stress state. Upon either tension or compression, the deformations of the U-shaped steel plates and disc springs are always consistent, owing to the assembled device. As the external force exceeds the preload of disc springs, the inner shaft begins to move relatively to the covering plates, which further compresses the disc springs and deforms the U-shaped steel plates. Gap is generated between the disc springs and block plates. The activated disc springs and deformed U-shaped steel plates provide SC and ED capacity for the brace, respectively. The deformation capacity of the brace is deemed consumed when the disc springs are fully flattened or the U-shaped steel plates reach to ultimate deformability.

The low-cycle fatigue behavior of the brace depends on that of the U-shape steel plates. According to an experimental work (Jiao et al. 2015), the fatigue life of the U-shape steel plates is mainly affected by loading direction and loading amplitude, whereas is less affected by loading speed and initial temperature. Although fatigue loading test on the brace is beyond the scope of this research, it would be an interesting topic to address in future work. After a major earthquake, the condition of the U-shape steel plates can be inspected by removing the side plates, as illustrated in Step 5 of Fig. 1. If through-thickness ruptures are found in the steel plates, the U-shape steel plates should be replaced.

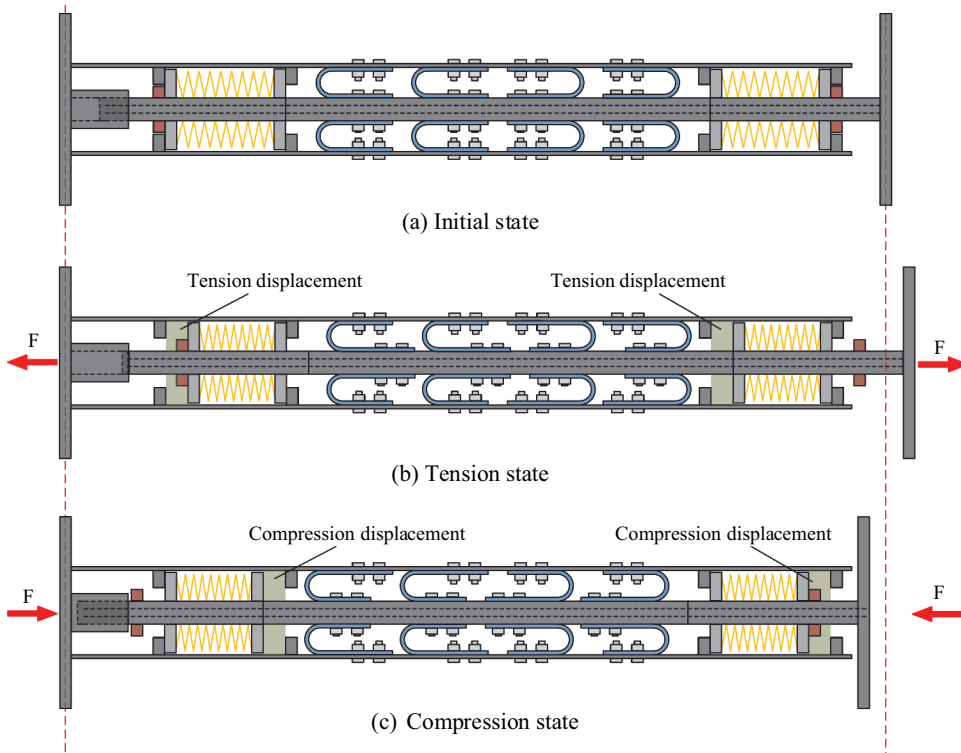


Figure 2. Working principle of the SCEDB-U.

3. Analytical Predictions

According to the working principle, the cyclic behavior of the SCEDB-U equals to the composition of the individual behavior of the U-shaped steel plates and pre-pressed disc springs. As schematically shown in Fig. 3, the idealized behaviors of the U-shaped steel plates, the pre-pressed disc springs and the SCEDB-U are assumed to be bilinear elastoplastic hysteresis, bilinear elastic hysteresis, and flag-shaped (FS) hysteresis, respectively. Detailed descriptions of the U-shaped steel plate, the pre-pressed disc spring and the SCEDB-U are separately elaborated in the following sections.

3.1. Analytical Behavior of U-Shaped Steel Plate

Figure 4 schematically shows the basic form and deformed shape of a single U-shaped steel plate. It includes the upper and lower straight segment and semicircle segment. The U-shaped steel plate is usually fabricated by bending a rectangular plate. The critical geometric parameters include the length of straight segment (L), overall height (h), overall width (b), plate thickness (t) and radius of semicircle segment (R). The parameter of l , which measures the distance from the dividing line between the semicircular and straight segments to the nearest bolt hole, represents the deformation capacity of the U-shaped steel plate. Hence, the allowable stroke of the brace is up to $2l$. As the U-shaped steel plate is deformed, the bending moment would cause the critical section to gradually develop from the elastic stage into fully plastic stage (Deng, Pan, and Wang 2013). Meanwhile, the yielding section continuously changes with the applied deformation.

As indicated in Fig. 3a, the hysteretic behavior of the U-shaped steel plate is simplified as a bilinear elastoplastic model. In this figure, F_{ey} is the yielding strength and u_{ey} is the yielding displacement; k_{e1} is

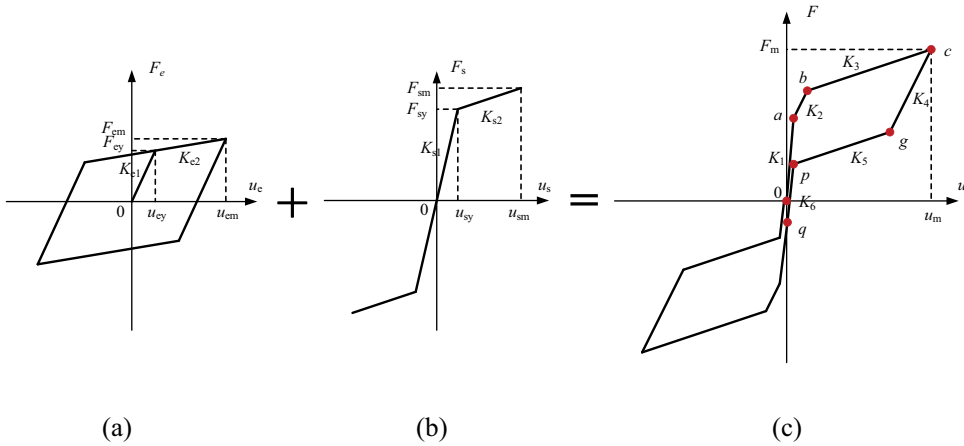


Figure 3. Idealized behaviors (not to scale): (a) U-shaped steel plates; (b) pre-pressed disc springs; (c) SCEDB-U.

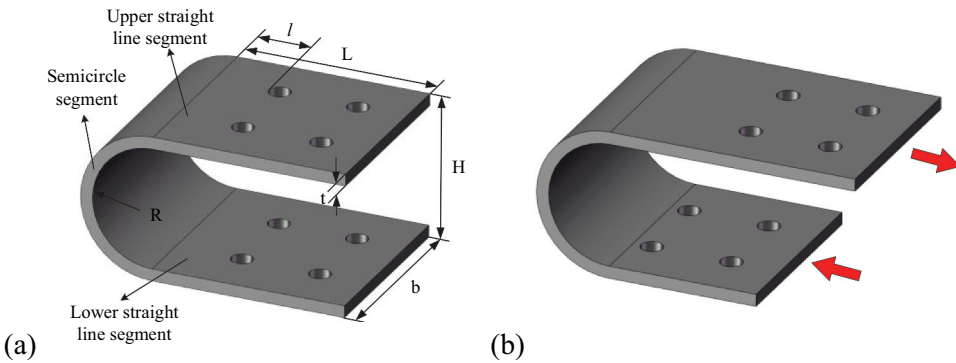


Figure 4. U-shaped steel plate: (a) basic form; (b) deformed shape.

the initial elastic stiffness and k_{e2} is the post-yielding stiffness. By considering the strain hardening of steel, the yielding strength of the U-shaped steel plates is calculated by Qu et al. (2019):

$$F_{em} = n \frac{2B\lambda}{R^{\gamma}(\gamma + 2)R} \left(\frac{T}{2}\right)^{\gamma+2} \quad (1)$$

where, λ and γ are the material cyclic loading parameter. If the Q235 steel is used, λ and γ take 719.8 and 0.111, respectively (Qu et al. 2019).

However, it is very challenging to calculate the initial stiffness and it still remains unknown in existing studies (Deng et al. 2015; Deng, Pan, and Wang 2013; Jiao et al. 2015; Qu et al. 2019; Taiyari, Mazzolani, and Bagheri 2019). In fact, the initial stiffness of the U-shaped steel plate is quite small, in comparison to the other types of steel dampers. Moreover, as will be shown in the following experimental work, the initial stiffness of the U-shaped steel plates is found considerably smaller than that of the pre-pressed disc springs, inner shaft, and covering plates. Hence, the initial and yielding stiffness of the U-shaped steel plates are ignored in the analytical equations. In other words, it assumes the U-shaped steel plates only provide strength and damping for the SCEDB-U. Detailed discussions on U-shaped steel plates can be found in earlier studies (Deng et al. 2015; Deng, Pan, and Wang 2013; Jiao et al. 2015; Qu et al. 2019; Taiyari, Mazzolani, and Bagheri 2019).



Figure 5. Disc spring: (a) basic form; (b) stacked in parallel; (c) stacked in series.

3.2. Analytical Behavior of Disc Spring

The schematic of a single disc spring is shown in Fig. 5. In this paper, 75% of the flattening height of disc springs is taken as the limit displacement, which is to ensure that disc springs remain elastic within the target deformation. Figure 5a shows basic form of a disc spring. The geometric configuration of a typical disc spring is characterized by the following parameters: external and internal diameters (D and d ; defining $C = D/d$), height (H_0), and thickness (t'). Figure 5b,c demonstrate that a group of disc springs can be used with different stack combinations, i.e. in series or in parallel, to achieve flexible deformability and load resistance, respectively. Compared with other types of springs, such as helical or friction springs, the disc springs are more stable due to their flat annular conical shape and concentric force transmission. The relationship between the load resistance F and the compressive deformation f can be expressed by (GB T1972–2005 2005):

$$F(f) = \frac{4E}{1 - \mu^2} \times \frac{t'^4}{K_1 D^2} \times K_4^2 \times \frac{f}{t'} \left[K_4^2 \left(\frac{h'_0}{t'} - \frac{f}{t'} \right) \left(\frac{h'_0}{t'} - \frac{f}{2t'} \right) + 1 \right] \quad (2)$$

where E = Young's modulus of the material; μ = Poisson's ratio; and h'_0 = maximum deformation capacity of each disc spring, as expressed:

$$h'_0 = H_0 - t' \quad (3)$$

Other parameters can be obtained by the following equations:

$$K_1 = \frac{1}{\pi} \times \frac{[(C - 1)/C]^2}{(C + 1)(C - 1) - 2/\ln C} \quad (4)$$

$$K_4 = \sqrt{-\frac{C_1}{2} + \sqrt{\left(\frac{C_1}{2}\right)^2 + C_2}} \quad (5)$$

$$C_1 = \frac{\left(\frac{t'}{t}\right)^2}{\left(\frac{5}{8} \times \frac{H_0}{t} - \frac{t'}{t} + \frac{3}{4}\right) \left(\frac{5}{8} \times \frac{H_0}{t} - \frac{t'}{t} + \frac{3}{8}\right)}, \frac{t'}{t} = 0.94 \quad (6)$$

$$C_2 = \frac{C_1}{(t'/t)^3} \left[\frac{5}{32} \left(\frac{H_0}{t} - 1 \right)^2 + 1 \right] \quad (7)$$

The tangent stiffness of the disc spring is given by:

$$K(f) = \frac{4E}{1 - \mu^2} \times \frac{t'^3}{K_1 D^2} \times K_4^2 \left\{ K_4^2 \left[\left(\frac{h'_0}{t'} \right)^2 - 3 \times \frac{h'_0}{t'} \times \frac{f}{t'} + \frac{3}{2} \left(\frac{f}{t'} \right)^2 \right] + 1 \right\} \quad (8)$$

3.3. Analytical Behavior of the SCEDB-U

Since the individual behaviors of the U-shaped steel plates and pre-pressed disc springs have been derived, the behavior of the brace can be readily obtained. As shown in Fig. 3c, the behavior of the brace is idealized as a FS hysteresis. Because the brace has a symmetrical arrangement, this subsection only takes the tension state for deriving the force-deformation relationship. A stage-by-stage description of the full behavior under tensile loading cycle is given as below:

1) The first stage under loading (*oa* section in Fig. 3c). The brace deforms under the applied load, whereas the load is insufficient to trigger the relative movement between the inner shaft and covering plates. The disc springs still firmly contacts with the block plates, and the U-shaped steel plates do not deform. At this stage, the elastic stiffness, K_1 , the restoring force, F_{oa} , and the force and displacement at point *a*, F_a and u_a , are calculated by:

$$K_1 = \frac{K_{in}K_{out}}{K_{in} + K_{out}} + K_{e1} + K_s \approx \frac{K_{in}K_{out}}{K_{in} + K_{out}} + K_s \quad (9)$$

$$F_{oa} = K_1 u_{oa} \quad (10)$$

$$F_a = F_0, u_a = \frac{F_0}{K_1} \quad (11)$$

where K_{in} , K_{out} , K_s and K_{e1} are the axial stiffness of inner shaft, covering plates, disc springs, and elastic stiffness of the U-shaped plates, respectively; F_0 is the pre-pressed amplitude of the disc springs.

2) The second stage under loading (*ab* section in Fig. 3c). The applied load keeps increasing and exceeds the pre-pressure of the disc springs, which drives the inner shaft to slide relatively to the covering plates. The disc springs are further compressed, whereas the U-shaped steel plates remain elastic. The stiffness at this stage is provided by the disc springs and U-shaped steel plates. At this stage, the stiffness, K_2 , the restoring force, F_{ab} , and the displacement and force at point *b*, u_b and F_b , are calculated by:

$$K_2 = K_{e1} + K_s \approx K_s \quad (12)$$

$$F_{ab} = F_a + K_2(u_{ab} - u_a) \quad (13)$$

$$u_b = u_{ey}, \quad F_b = F_a + K_2(u_b - u_a) \quad (14)$$

where u_{ey} is the yielding displacement of the U-shaped steel plates. According to earlier studies (Deng et al. 2015; Deng, Pan, and Wang 2013), u_{ey} is small. Hence, the displacement increment from u_a to u_b is minimal, which implies that the values of F_a and F_b are very close.

3) The third stage under loading (*bc* section in Fig. 3c). With the increasing of external load, the U-shaped steel plates begin to yield, and the stiffness at this stage is provided by the disc springs and yielding stiffness of the U-shaped steel plates. The deformation capacity of the SCEDB-U is determined by the smaller value of the deformation capacity of U-shaped steel plates and disc springs, which is controlled by l and δ_f , respectively. At this stage, the stiffness, K_3 , the restoring force F_{bc} and the displacement and force at point *c*, u_c and F_c , are calculated by:

$$K_3 = K_{e2} + K_s \approx K_s \quad (15)$$

$$F_{bc} = F_b + K_3(u_{bc} - u_b) \quad (16)$$

$$u_c = \min\{l, \delta_f\}, F_c = F_b + K_3(u_c - u_b) \quad (17)$$

4) The first stage under unloading (*cg* section in Fig. 3c). It begins to remove the applied load. At this stage, the U-shaped steel plates are elastic. The unloading path corresponds to a hysteresis width of $2F_{ey}$. The total stiffness is provided by elastic stiffness of the covering plates, the U-shaped steel plates and disc springs. At this stage, the stiffness, K_4 , the restoring force, F_{cg} , and the displacement and force at point *g*, u_g and F_g , are calculated by:

$$K_4 = \frac{K_{in}K_{out}}{K_{in} + K_{out}} + K_{e1} + K_s \approx \frac{K_{in}K_{out}}{K_{in} + K_{out}} + K_s \quad (18)$$

$$F_{cg} = F_c - K_4(u_c - u_{cg}) \quad (19)$$

$$u_g = u_c - 2u_{ey}, F_g = F_c - 2K_4u_{ey} \quad (20)$$

5) The second stage under unloading (*gp* section in Fig. 3c). The yielded U-shaped steel plates and compressed disc springs begin to recover deformation. This stage is like the *bc* section, and the stiffness is the same as K_3 . At this stage, the stiffness, K_5 , the restoring force, F , and the displacement and force at point *p*, u_p and F_p , are calculated by:

$$K_5 = K_3 = K_{e2} + K_s \approx K_s \quad (21)$$

$$F_{gp} = F_d - K_5[u_d - u(t)] \quad (22)$$

$$u_p = u_a, \quad F_p = F_g - K_5(u_g - u_p) \quad (23)$$

6) The third stage upon unloading (*po* section in Fig. 3c). This is the final stage in a full loading cycle. At this stage, the inner shaft and covering plates contact again, and the unloading displacement is very small. Theoretically, compared with the first stage during loading, the current stiffness is slightly small, because the U-shaped steel plates are in plastic state. At this stage, the stiffness, K_6 , the restoring force, F_{op} , and the force at point *q*, F_q , are calculated by:

$$K_6 = \frac{K_{in}K_{out}}{K_{in} + K_{out}} + K_{e2} + K_s \approx \frac{K_{in}K_{out}}{K_{in} + K_{out}} + K_s \quad (24)$$

$$F_{pq} = F_p - K_6[u_p - u(t)] \quad (25)$$

$$u_q = 0, \quad F_q = F_p - K_6(u_p - u_q) \quad (26)$$

3.4. Major Design Considerations

Besides with strength and stiffness, for the SCEDB, the damping capability and recentering capacity are additional major design considerations. To maximize energy absorbing capacity, the brace is required to have a full hysteresis, and meanwhile, to ensure the brace could completely recover deformation, the brace should have a perfect recentering behavior. However, the readers should be aware that, under earthquake-induced dynamic loading conditions, the above requirement seems to be stringent. According to recent studies (Qiu, Cheng, and Du 2022; Zhang et al. 2022; Zhang, Wang, and Alam 2022), a hysteresis between typical bilinear elasto-plastic behavior and FS behavior, which is deemed as a partial SC behavior, seems to be more desirable, because it performs better in simultaneous control of the peak deformation, residual deformation, and peak floor acceleration. Although the partial SC behavior could lead to minimal residual deformation from a probabilistic sense, an unconditional SC behavior can be achieved when it satisfies $F_p = 0$. As shown in Fig. 3c, F_p is further expressed as:

$$F_p = F_0 - F_{ey} - K_{e1}u_{sy} + K_{e2}(u_{ey} + u_{sy}) \quad (27)$$

where the values of u_{sy} and u_{ey} are small and can be ignored. Hence, F_p can be approximated by:

$$F_p = F_0 - F_{ey} \quad (28)$$

which indicates that when the pre-pressure of the disc springs is greater than the yield strength of the U-shaped steel plates, the residual deformation equals to zero. However, the above derivation is based on the simplified model. In fact, steel is prone to experience isotropic hardening under repeated cyclic loadings (Rossi 2015), which leads to a higher yielding strength in the successive loops. Therefore, to ensure the brace could consistently recenter to original position, it is suggested that the pre-pressure of disc springs should be greater than the yield strength of the U-shaped steel plates, i.e. $F_0 > \omega F_{ey}$ ($\omega > 1$). In this work, the ω is assumed to be 1.2.

4. Experimental Tests

4.1. Overview

In order to obtain the hysteretic behavior of the SCEDB-U under axial cyclic loadings, the quasi-static tests of the full-scale SCEDB-U specimens were carried out. The testing matrix is shown in Table 1. The SC system (pre-pressed disc springs), ED system (U-shaped steel plates) and the stacked system (SCEDB-U) were tested in sequence. All systems were tested using the same loading device. Firstly, the disc springs were tested to confirm the recentering capability and to assess the effect of changing initial preload magnitude. Secondly, the U-shaped steel plates were tested to obtain the damping capacity and to explore the influence of changing the width of steel plates. Finally, the SCEDB-U was fabricated by assembling the SC and ED systems together and then subjected to loading cycles. For the SCEDB-U, the varied parameters included the plate width of U-shaped steel plates and the initial preload magnitude of disc springs. In summary, there are 11 testing cases, including 3, 3 and 5 cases for the SC, ED and combined systems, respectively.

4.2. Specimens

Figure 6 shows the large-scale specimens of the SCEDB-U. The specimen has a global length of 2870 mm and a cross section of 600 mm × 600 mm. Stiffening ribs were welded along the inner shaft and covering plates to enhance global stability. To avoid potential contact that may induce friction force, a 5 mm space was reserved between the inner shaft and covering plates. Similarly, the block plates of the disc springs were also shifted away from the covering plates by 5 mm. The straight segments of the U-shaped steel plates were bolted with the inner shaft and covering plates through high-strength bolts with grade 8.8 M16 (diameter = 13.4 mm, nominal tensile strength = 400 MPa). Being consistent with the design concept, two groups of disc springs were symmetrically arranged at both ends of the brace.

Table 1. Testing matrix of the SCEDB-U.

Description	Notation	Pre-pressure of disc springs (F/kN)	Width of U-shaped steel plates (B/mm)
SC system/ Pre-pressed disc springs	F160	160	—
	F200	200	—
	F240	240	—
ED system/ U-shaped steel plates	B120	—	120
	B160	—	160
	B200	—	200
Combined system/ SCEDB-U	F160-B160	160	160
	F200-B120	200	120
	F200-B160	200	160
	F200-B200	200	200
	F240-B160	240	160

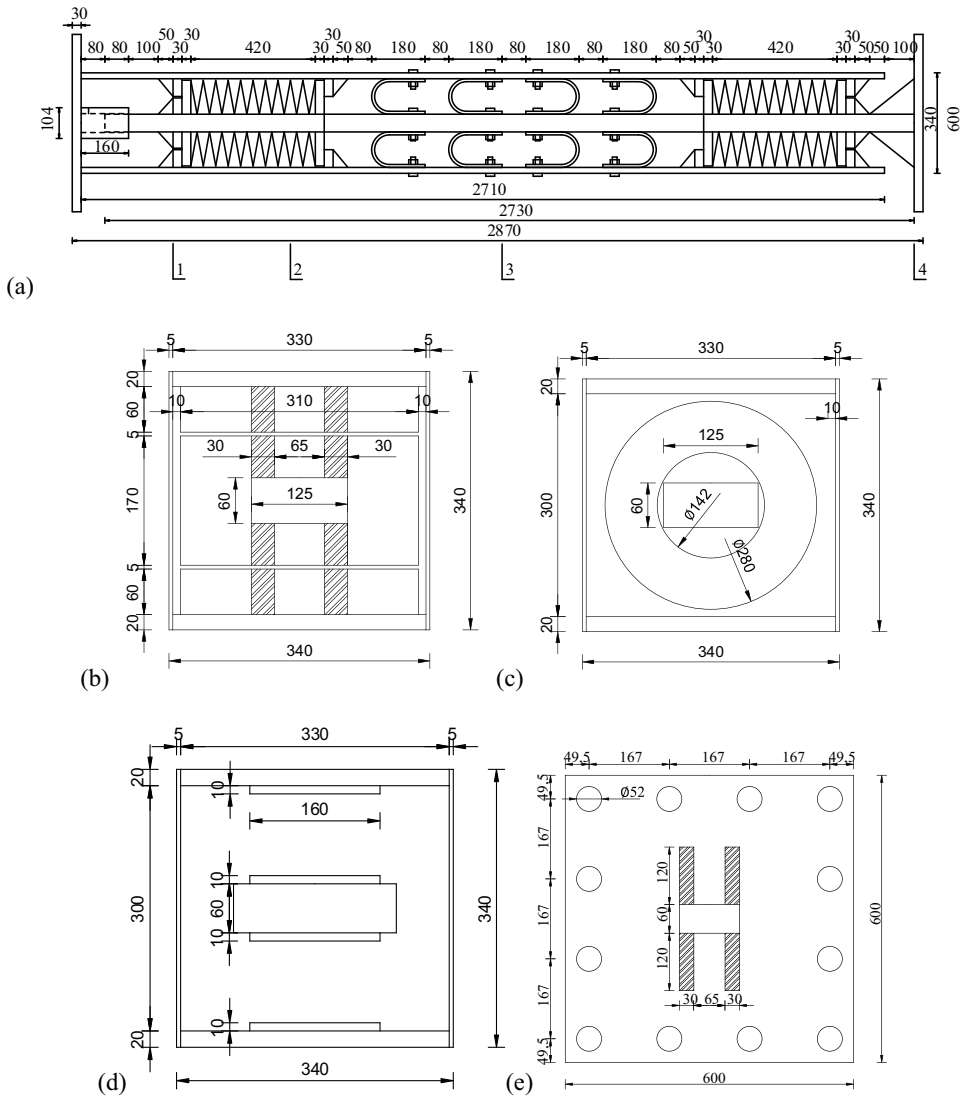


Figure 6. Large-scale specimen of the SCEDB-U: (a) overall dimension (mm); (b) section 1-1; (c) section 2-2; (d) section 3-3; (e) section 4-4.

As the SC system, the disc springs were firstly tested. This test adopted the disc springs in category 3 with the supporting surface of A series, according to the Chinese standard (GB T1972-2005 2005). The supporting surface can increase its bearing area and reduce the friction between the inner shaft and disc springs. The disc springs were made of 60Si2MnA steel (Chinese Standard 2005). The outer diameter of disc spring was $D = 280$ mm, the inner diameter was $d = 142$ mm, the thickness was $t' = 14.75$ mm, the free height of a single disc spring was $H_0 = 22$ mm, and the maximum compression deformation of a single disc spring was $H_0' = 7.25$ mm. To explore the influence of disc spring's initial pre-pressure on SC ability of the brace, three magnitudes of initial pre-pressure of were considered, including 160 kN, 200 kN and 240 kN. Accordingly, the specimens were denoted as F160, F200 and F240, respectively.

In what followed, the disc springs were dismantled from the bracing device and the U-shaped steel plates were installed. As the ED system, all U-shaped steel plates were made of Q235 steel (nominal

yield strength = 215 MPa). Each one had a height of $H = 120$ mm, a total length of $L = 180$ mm, a radius of $R = 60$ mm, and a plate thickness of $t = 10$ mm. The theoretical maximum deformation of the U-shaped steel plates was 142 mm. The configuration and testing manner of ED system were similar to that presented in Qu et al. (2019). To explore the influence of the width of the U-shaped steel plates on ED capacity, three steel plate widths were considered, including 120 mm, 160 mm, and 200 mm, and the corresponding yielding strengths are estimated to be 207, 276 and 345 kN, respectively. Accordingly, the specimens were denoted as B120, B160 and B200, respectively.

After the SC and ED systems have been separately investigated, they were combined together to achieve the SCEDB-U specimens. A total of 5 specimens were designed, fabricated and tested, depending on the various combinations of disc springs with different preload magnitudes and U-shaped steel plates with different plate width. Specifically, to assess the effect of changing the width of U-shaped steel plates, the pre-pressure of the disc springs was maintained to be 200 kN, and the width of U-shaped steel plate included 120 mm, 160 mm, and 200 mm; to assess the effect of changing preload magnitude, the width of U-shaped steel plate was maintained to be 160 mm, whereas the preload magnitude of disc springs included 160 kN, 200 kN, and 240 kN. Accordingly, the specimens were denoted as F160-B160, F200-B120, F200-B160, F200-B200, and F240-B160, respectively.

The specimens were designed for proof-of-concept purpose. Each individual disc spring can provide a theoretical maximum load resistance of 322.9 kN at the allowable deformation (≈ 5.4 mm), which is 75% of the maximum deformation capacity (≈ 7.25 mm). A total of 20 disc springs were stacked in series the current specimen. This combination allows a total allowable deformation of 108 mm and a maximum deformation capacity of 145 mm, among which 20.0, 25.2 and 30.6 mm were consumed for preloading values of 160, 200 and 240 kN, respectively. The remaining deformation capacity was used for axial deformation.

4.3. Material Tests on U-Shaped Steel Plates

Material properties of the U-shaped steel plates were obtained through coupon tests using monotonic tensile loading. The coupons were selected, manufactured, and tested according to the Chinese Standard (GB/T 228.1-2010 2010). Figure 7 shows the nominal dimension of the specimens for coupon test. Three specimens were tested and the average result was defined as the material properties of the steel. Table 2 summarizes the yield strength, F_y , the ultimate strength, F_u , the strain associated with the onset of hardening, ϵ_{sh} , and the maximum elongation at failure, δ , of the materials used in the U-shaped steel plates. Please note that the nominal and actual thicknesses of the steel plates were 10 and 10.2 mm, respectively.

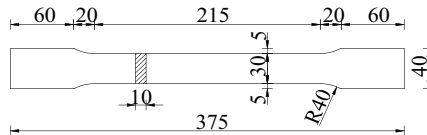


Figure 7. Nominal dimension of the specimen for coupon test (unit: mm).

Table 2. Average result from coupon test.

Steel	f_y /Mpa	f_u /Mpa	E /Gpa	ϵ_{sh}	$\delta\%$
Q235B	290.9	453.3	193	0.0134	27.70

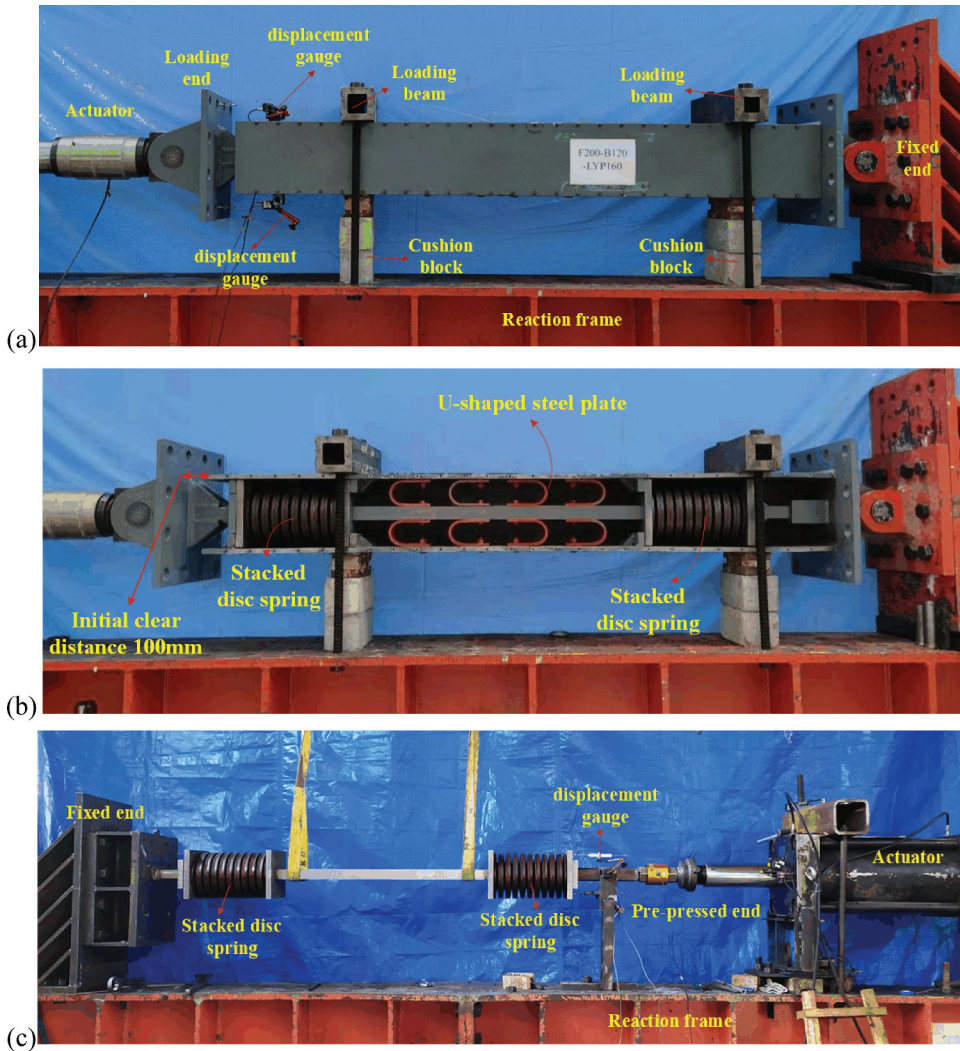


Figure 8. Experimental setup: (a) with side plates; (b) without side plates; (c) precompression of stacked disc springs.

4.4. Experimental Setup and Loading Scheme

Figure 8a shows the experimental setup, in which the specimen was mounted within a strong reaction frame and the loading was applied using a hydraulic servo actuator with a capacity of 2000 kN. For installation purpose, the ends of the specimen were welded with strong ear plates, which were then pinned to the actuator and reaction frame, respectively. The specimen was laid on supporting blocks to fit the height of the actuator. As shown in Figure 8b, to show the internal component and permit convenient observation, one side plate was removed from the brace during the tests. Figure 8c shows the precompression of stacked disc springs. The stacked disc springs were precompressed to the target deformation via an actuator, and then they were restricted by temporary blocks. After that, the upper and lower plates were installed and the temporary blocks were removed.

The selection of loading protocol remains an active research topic and it becomes even more challenging when a novel device is required to be tested. Extensive discussions can be found in Aguaguña, Zhou, and Zhou (2019) and Fang et al., (2020). In current work, a simple yet effective loading protocol was used to obtain the cyclic behavior of the brace, but using the other types of